IRANIAN JOURNAL OF CATALYSIS

A simple synthetic technique to produce $ZnO/Fe_2O_3/Fe_3O_4$ nanostructures and application as a photocatalyst

Nai-Feng Hsu[a]* and Kuei-Ting Hsu[b]

a)General Education Center, Army Academy, Chungli, Taiwan ROC

b) Department of Chemical Engineering, Army Academy, Chungli, Taiwan ROC

Received 28 September 2021; received in revised form 10 February 2022; accepted 21 February 2022

ABSTRACT

In this study, a simple technique was used for synthesizing one-dimensional $ZnO/Fe_2O_3/Fe_3O_4$ nanostructures (NSs) through heat treatment under vacuum by using a magnetic field at a temperature of 200 °C for 1 h. The photocatalytic effect of the NSs were studied by decomposing methyl orange (MO) dye (5 mg/L, pH = 8.1) under ultraviolet illumination. The experimental results indicated that a 33-mg/L $ZnO/Fe_2O_3/Fe_3O_4$ NS-containing film on glass could reduce the MO concentration by 37% in 100 min, and the synthesized $ZnO/Fe_2O_3/Fe_3O_4$ NS-containing films could be reused to degrade MO solution. Moreover, 0.1 g/L of $ZnO/Fe_2O_3/Fe_3O_4$ NS-containing powder exhibited an excellent photocatalytic effect and reduced the MO concentration by almost 90% in 100 min.

***Keywords**: ZnO/Fe₂O₃/Fe₃O₄ nanostructures; Heat treatment in vacuum; Magnetic field; Photocatalyst*

1. Introduction

Residential sewage, industrial waste, and dyes are among the leading causes of water pollution [1]. In particular, textile industries discharge large amount of dyeing sewage, which is resistant to biological degradation and degrades slowly. For the complete elimination of contaminants from effluents, advanced oxidation processes (AOPs) have been developed [2, 3]. However, AOPs are costly, and can eliminate the chemical reagents used in them is difficult [4–6]. Photocatalysis is a potential solution for wastewater treatment and can be used to achieve the complete mineralization of organic compounds with high efficiency [7]. Metal oxide nanomaterials, such as TiO_2, $BiVO_4$, Fe_2O_3, and ZnO, are nontoxic, stable, and cheap and exhibit high photocatalytic efficiency; thus, these materials can be used for treating wastewater [8–11]. One-dimensional nanostructures (NSs) have attracted considerable research attention because of their large surface-area-to-volume ratio and unique electrochemical properties [12].

*Corresponding author:
E-mail address: *nai-feng@aaroc.edu.tw* (**N. F. Hsu**)

ZnO and iron oxide nanomaterials are widely used in the field of nanotechnology [13]. Thus, ZnO and iron oxide NSs can be used as highly efficient photocatalyst materials for water treatment [14, 15]. ZnO and iron oxide NSs are grown using various techniques, including surfactant-free aqueous methods, hydrothermal processes, the vapor transport method, sputter deposition, laser ablation, the vapor–solid method, and solution-phase processes [16–24]. A simple two-step thermal oxidation method was proposed in [25] for rapidly synthesizing ZnO nanowires on a Si substrate. However, this method requires an operational temperature higher than 350 °C. In the present study, ZnO nanofibers and iron oxide NSs were synthesized on a wafer through a simple heat treatment process in vacuum by using a magnetic field for 1 h at 200 °C. Various metal oxide NSs can potentially be grown using this novel technique.

Methyl orange (MO) dye was used to study the catalytic efficiency of the prepared $ZnO/Fe_2O_3/Fe_3O_4$ NSs. The experimental results indicated that a 33-mg/L $ZnO/Fe_2O_3/Fe_3O_4$ NS-containing film on a glass substrate reduced the MO concentration by 37% in 100 min. The grown $ZnO/Fe_2O_3/Fe_3O_4$ NS-containing film could be reused for degrading MO solution.

Furthermore, 0.1 g/L of $ZnO/Fe_2O_3/Fe_3O_4$ NS-containing powder exhibited an excellent photocatalytic effect and reduced the MO concentration by 90% in 100 min.

2.Experimental

2.1. Preparation of $ZnO/Fe_2O_3/Fe_3O_4$ NS photocatalysts

Fig. 1 illustrates the synthesis of $ZnO/Fe_2O_3/Fe_3O_4$ NSs on a substrate (a 50 × 30 × 1-mm^3 SiO wafer or glass substrate). A total of 30 mg of zinc powder (purity of 99%; Shimakyu's Pure Chemicals Company, Japan) with a nanoparticle diameter of approximately 500 nm and 10 mg of iron powder (purity 99.0%; Shimakyu's Pure Chemicals Company) with a nanoparticle diameter of approximately 900 nm were mixed with 100 mL of a 0.75 mol/L oxalic acid solution in a 250-mL glass flask. This mixture was stirred in an ultrasonic oscillator for 10 min and then deposited dropwise using a syringe on a substrate, which was then set on a specially fabricated quartz plate (height of 25 mm) at a distance of 5 mm from a magnet placed on the plate. The plate was then placed inside a quartz tube furnace (Olink, OT-060-30) and heated to 150 °C over 5 min at a constant heating rate of 30 °C/min to create a thin-film substrate. The substrate was heated to 200 °C. Subsequently, the tube was vacuumed, and heating was continued for 1 h. Finally, the substrate was allowed to cool to room temperature to create an approximately 1 mg $ZnO/Fe_2O_3/Fe_3O_4$ NS-containing film on the substrate. In the aforementioned synthesis process, the magnet (50 × 30× 20 mm^3) had a magnetic flux density (*B*) of 430 G.

3. Results and Discussion

3.1. Synthesis and characteristics of $ZnO/Fe_2O_3/Fe_3O_4$ NSs

In the adopted synthesis process, $ZnC_2O_4 \cdot 2H_2O$ and $FeC_2O_4 \cdot H_2O$ compounds were formed when the temperature of the substrate fell below 190 °C, above which the compounds gradually were transformed into ZnO and iron oxide layers [26], which became unstable as atoms diffused out from them as the temperature increased [27, 28]. The atoms obtained energy for outward diffusion from the thin-film layer being subject to heat treatment. The iron atoms simultaneously struck other atoms when diffusing outward to form NSs because of the applied magnetic field; thus, one-dimensional $ZnO/Fe_2O_3/Fe_3O_4$ NSs were formed at 200 °C. The corresponding chemical reaction can be expressed as follows:

$$2Zn + 4Fe + 3O_2 + 6H_2C_2O_4 \rightarrow 2ZnC_2O_4 + 4FeC_2O_4 + 6H_2O \quad (1)$$

$$ZnC_2O_4 + 5FeC_2O_4 \rightarrow ZnO + Fe_2O_3 + Fe_3O_4 + 8CO + 4CO_2 \quad (2)$$

Fig. 2(a) displays the scanning electron microcopy (SEM) image of the nanofibers produced on the wafer substrate at a temperature of 200 °C after 20 min of the reaction. The average length and diameter of these nanofibers were approximately 400 and 75 nm, respectively. **Fig. 2(b)** indicates that the number of nanofibers formed increased over 1 h, and the nanofibers formed a honeycomb shape. **Fig. 2(c)** depicts a magnified SEM image of the nanofibers shown in **Fig. 2(b)**. **Fig. 2(d)** presents the SEM image of nanorods alone. **Fig. 3** illustrates the results of energy-dispersive X-ray spectroscopy (EDS) analysis. **Fig 3(a)** indicates that the O:Si atomic ratio was 51:49 (close to 1:1); thus, the substrate contained a SiO wafer. **Fig. 3(b)** indicates that the O:Si atomic ratio was 48:24 (the O:Si:Zn atomic ratio was 48:24:28); thus, the nanofibers grown on the substrate [in **Fig. 2(c)**] might have contained Zn and O. As displayed in **Fig. 3(c),** the O:Si atomic ratio of the nanorods was 52:31 (the O:Si:Fe atomic ratio was 52:31:17); thus, the nanorods synthesized on the substrate [in **Fig. 2(d)**] might have been iron oxide products. The Fe_3O_4 nanorods formed a quadrangular pattern [29]. Thus, the nanorods [red circle in **Fig. 2(b)**] were potentially a Fe_3O_4 structure. Moreover, the Fe_3O_4 nanomaterials aggregated under an external magnetic field [30]. SEM-EDS analysis indicated that the honeycomb-shaped NSs were ZnO crystals and that the nanorods comprised FeO, Fe_3O_4, or Fe_2O_3.

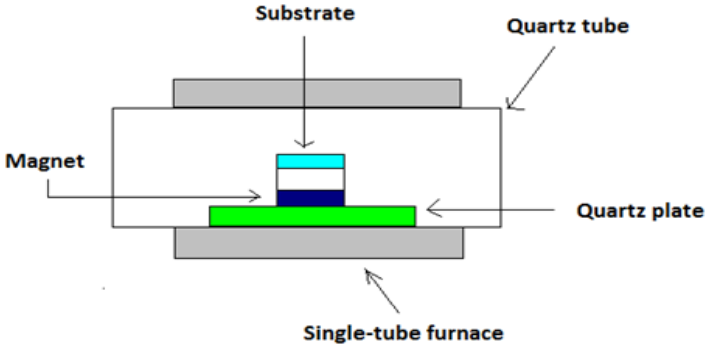

Fig. 1. Experimental equipment used for growing $ZnO/Fe_2O_3/Fe_3O_4$ NSs.

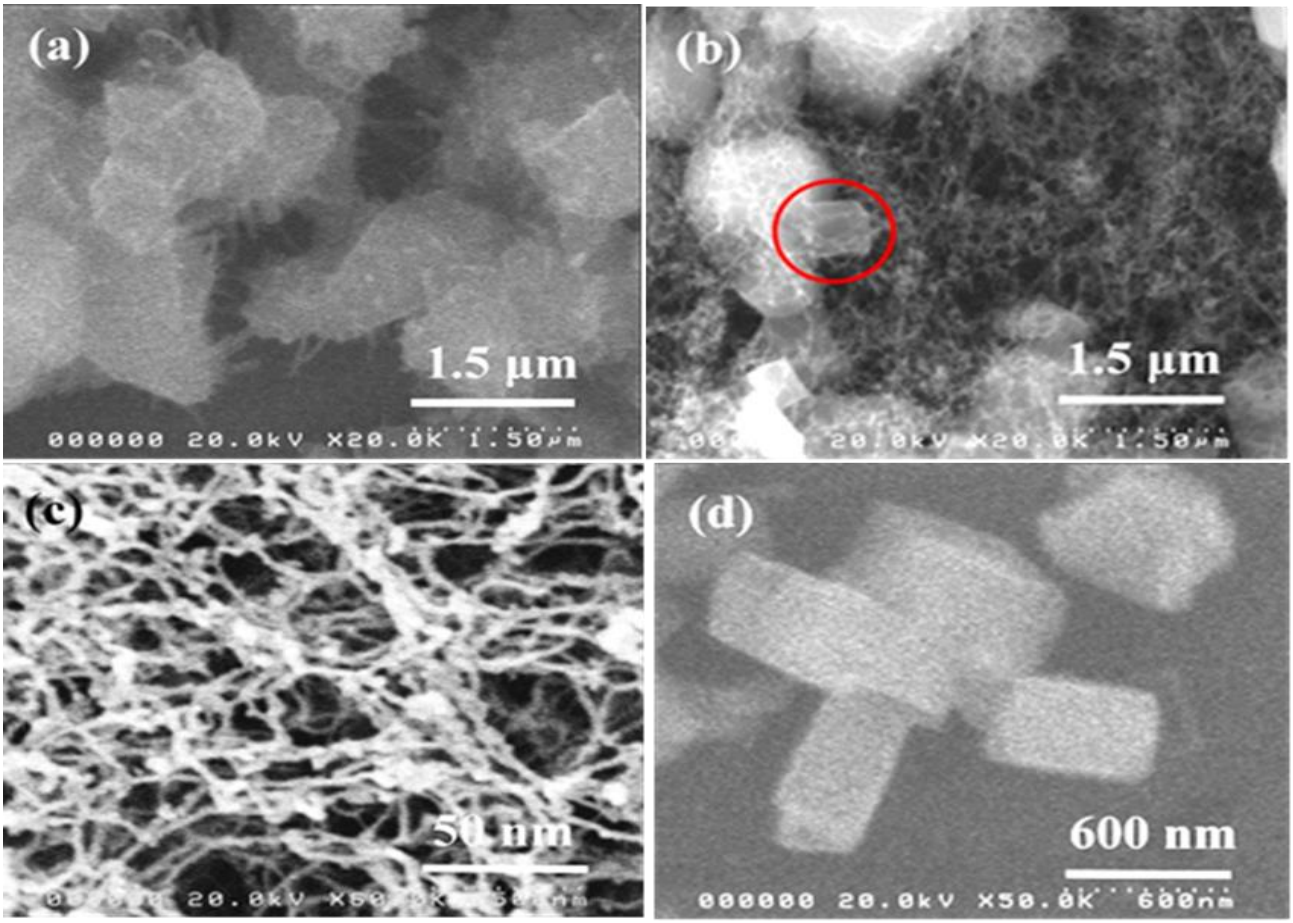

Fig. 2. SEM image of the $ZnO/Fe_2O_3/Fe_3O_4$ NSs grown on a SiO substrate at 200 °C for (a) 20 min and (b) 1 h, (c) magnified SEM image of the honeycomb shape in Fig. 3(b), and (d) SEM image of the prepared nanorods.

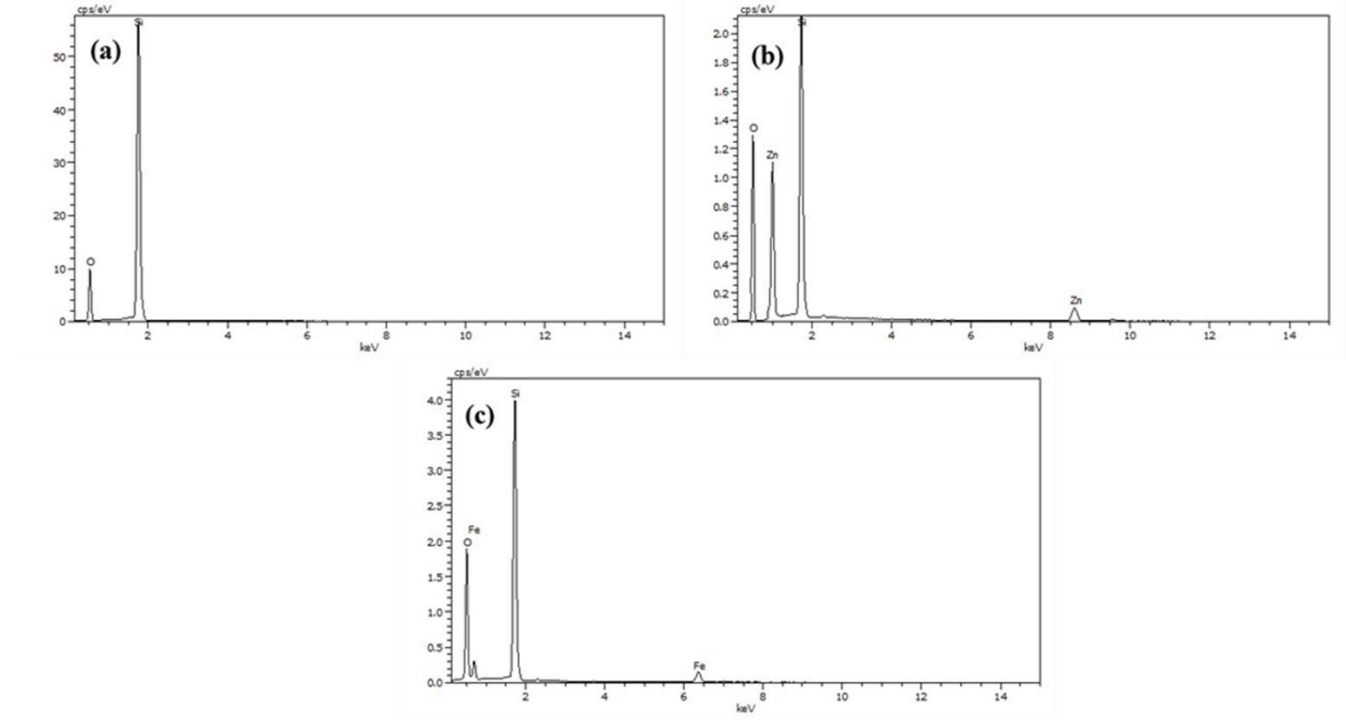

Fig. 3. EDS spectra of the (a) SiO wafer, (b) ZnO NSs grown at 200 °C for 1 h, and (c) iron oxide NSs grown at 200 °C for 1 h.

Fig. 4 displays the X-ray diffraction (XRD) patterns of the products synthesized at different temperatures. **Fig. 4(a)** indicates that the mixed solution that was deposited on a glass substrate and dried at 150 °C for 5 min in air contained ZnC_2O_4•$2H_2O$ (JCPDS: 14-0740), FeC_2O_4 (JCPDS: 14-0807), Zn (JCPDS: 01-1244), Fe (JCPDS: 01-1267), and Fe_2O_3 (JCPDS: 47-1409). **Fig. 4(b)** illustrates the XRD patterns of the products synthesized at 200 °C for 1 h. The XRD peaks in **Fig. 4(b)** are different from those in **Fig. 4(a),** which indicates that the reaction products changed during the synthesis process. The peaks at 26.3°, 33.7°, and 62.7° indicate that the nanofibers comprised ZnO crystals (JCPDS: 21-1486). The peaks at 30.1° and 62.6° suggest that the nanorods comprised Fe_3O_4 crystals (JCPDS: 11-0614), and the peaks at 14.9°, 27.7°, and 40.3° can be attributed to Fe_2O_3 crystals (JCPDS: 15-0615). Fe_2O_3 and Fe_3O_4 were simultaneously synthesized through the thermal oxidation of FeC_2O_4 [29]. The aforementioned results indicate that the synthesized NSs comprised $ZnO/Fe_2O_3/Fe_3O_4$. One overlapping peak at approximately 67° was observed for ZnO and Fe_3O_4. This observation can be attributed to the similar ionic radii of Fe^{2+} and Zn^{2+} (0.076 nm) [31].

Fig. 5(a) displays the photoluminescence (PL) spectrum of $ZnO/Fe_2O_3/Fe_3O_4$ NSs, which was obtained using a He-Cd laser (λ = 260 nm) for illumination at room temperature (25 °C). First, the small full width at half maximum (FWHM) of the ultraviolet (UV) emission peak near 380 nm indicates that high-quality $ZnO/Fe_2O_3/Fe_3O_4$ NSs were synthesized at an operating temperature of 200 °C for 1 h [32]. Second, the products synthesized at an operating temperature of 200 °C for 20 min exhibited a large FWHM at the UV emission peak near 370 nm, which indicates that these products were poorly crystallized and that $ZnC_2O_4 \cdot 2H_2O$ and $FeC_2O_4 \cdot H_2O$ were not completely converted into $ZnO/Fe_2O_3/Fe_3O^4$ NSs. Furthermore, the wide emission band in the visible light area is ascribed to the overlap of green and yellow emissions [33, 34]. The green emission is typically associated with oxygen vacancies [35], whereas the yellow emission is associated with interstitial oxygen [36]. The results indicate that the $ZnO/Fe_2O_3/Fe_3O_4$ NSs grown at 200 °C for 1 h exhibited high crystal quality as well as oxygen vacancies and interstitial oxygen on their surfaces. The separation rate of electron–hole pairs increases with the number of oxygen defects (i.e., oxygen vacancies and oxygen interstices) [37]. Therefore, an increase in the surface defects of the $ZnO/Fe_2O_3/Fe_3O_4$ NSs resulted in an increase in their photocatalytic efficiency [38–40]. **Fig. 5(b)** depicts the hysteresis loops calculated for the $ZnO/Fe_2O_3/Fe_3O_4$ NSs through vibrating sample magnetometry, in which the magnetic field was applied perpendicular to the substrate. These loops exhibited a squareness (M_r/M_s) of approximately 0.27 and a coercive field (Hc) of approximately 217 Oe. These results reveal that the synthesized iron oxide NSs exhibited ferromagnetic behavior at room temperature.

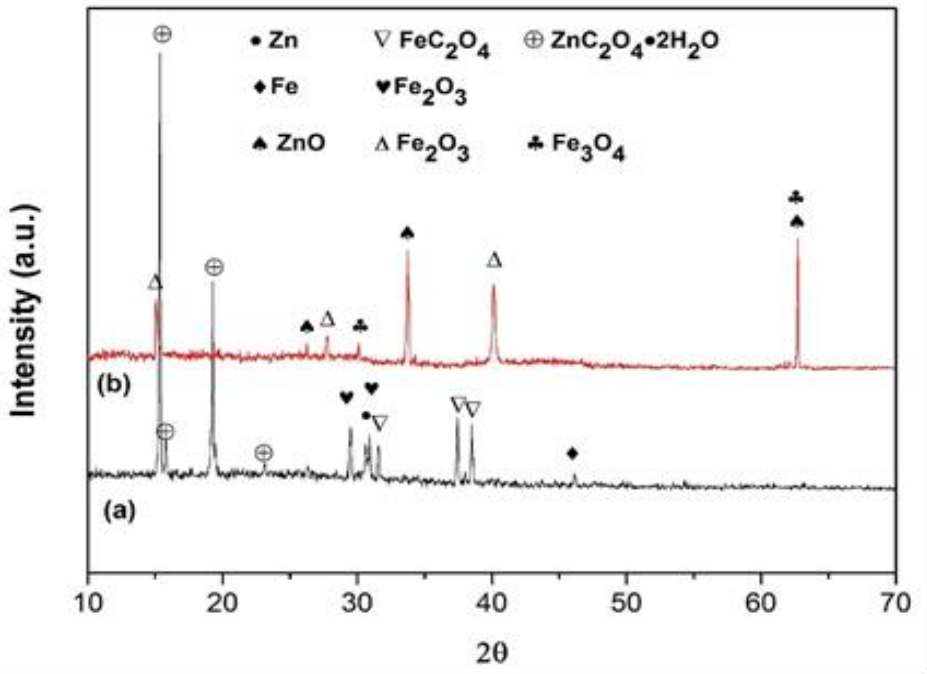

Fig. 4. (a) XRD pattern of the thin film obtained from the mixed solution deposited on a SiO substrate and dried at 150 °C for 5 min in air and (b) XRD patterns of the ZnO, Fe_2O_3, and Fe_3O_4 NSs grown at 200 °C for 1 h.

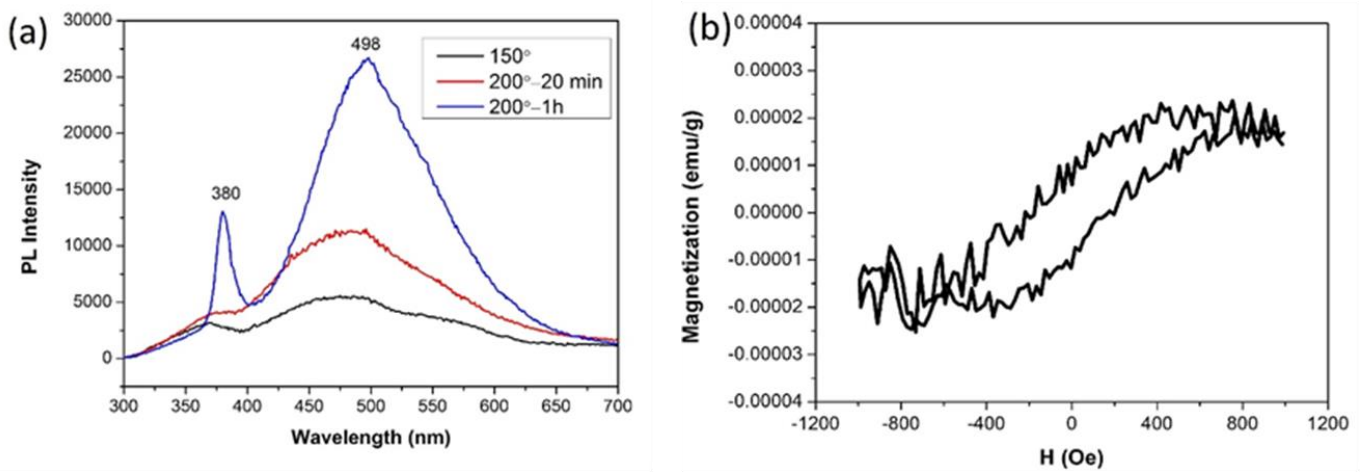

Fig. 5. (a) Typical PL spectra of the $ZnO/Fe_2O_3/Fe_3O_4$ NSs grown at 200 °C for 1 h and (b) hysteresis loop of the $ZnO/Fe_2O_3/Fe_3O_4$ NSs synthesized at 200 °C for 1 h.

3.2. Photocatalytic behavior of $ZnO/Fe_2O_3/Fe_3O_4$ NSs

3.2.1 MO removal

In this study, the photocatalytic effect of the synthesized $ZnO/Fe_2O_3/Fe_3O_4$ NSs was evaluated using the NSs as a photocatalyst in the decomposition of MO under UV illumination. Tests were conducted in a 50-mL glass measuring flask vacuumed to a closed structure under nitrogen. The concentration of the prepared MO solution was 5 mg/L (pH = 8.1). This solution was constantly mixed using a magnetic blender and irradiated using a 160-W mercury lamp for 100 min. The MO solution was maintained at 25 °C by using cooling equipment. The MO degradation efficiency was calculated as follows [41]:

$$\text{Degradation (\%)} = [(A_0 - A_t)/A_0] \times 100 \quad (3)$$

where A_0 represents the initial absorbance of the solution and A_t denotes the absorbance of the solution after t min of illumination.

Test 1 was performed on an MO solution that contained a 3 contained a $ZnO/Fe_2O_3/Fe_3O_4$ NS-containing film with a concentration of approximately 33 mg/mL (concentration of MO = 5 mg/L, pH of the solution = 8.1) synthesized on a glass substrate in the dark for 100 min. The reusability of the $ZnO/Fe_2O_3/Fe_3O_4$ NS-containing film was determined through the photocatalytic degradation of MO for three continuous cycles. After each cycle, the catalyst film was washed with deionized water through overnight drying in an oven at 60 °C. **Figs. 6(a)–6(c)** illustrate the absorption spectra of the MO solution for the first, second, and third degradation cycles, respectively. The absorption intensity of the MO solution decreased with the illumination duration, and the maximum absorbance occurred at a wavelength of approximately 461 nm. The MO degradation rates of the film containing $ZnO/Fe_2O_3/Fe_3O_4$ NSs were 37.1%, 32.5%, and 31.7% during the first, second, and third degradation cycles, respectively. The experimental results indicated that the aforementioned film could reduce the MO concentration by 37.1% in 100 min and that the film could be reused for MO degradation. However, the MO degradation rate decreased with repeated film use. A glass substrate with the same size as a magnet (50 × 30 mm^2) can only be used to synthesize an approximately 1 mg $ZnO/Fe_2O_3/Fe_3O_4$ NS-containing film. This film can only degrade 37.1% of 30 mL of MO solution. In Test 1, the MO degradation rate decreased from 37.1% to 31.7% over three degradation cycles. This result can be attributed to the loss of NSs during the experiment. The wafer may be turned over by the magnetic blender, which results in the NSs not being irradiated by UV light. Thus, the $ZnO/Fe_2O_3/Fe_3O_4$ NS-containing film was synthesized on a glass substrate in Test 1.

Test 2 was performed on six MO solutions (concentration = 5 mg/L, pH = 8.1), namely one MO solution without $ZnO/Fe_2O_3/Fe_3O_4$ NS-containing powder and five MO solutions containing 0.1 g/L $ZnO/Fe_2O_3/Fe_3O_4$ NS-containing powder (NSs were grown on a wafer and separated from it), in the dark for 100 min. **Fig. 6(d)** shows the absorption spectrum of the MO solution containing 0.1 g/L $ZnO/Fe_2O_3/Fe_3O_4$ NS-containing powder under 100-min UV illumination. The absorption intensity of the MO solution decreased with the illumination duration, and the maximum absorbance occurred at a wavelength of approximately 461 nm. Fig. 6(e) displays the MO degradation of five MO solutions containing 0.1 g/L $ZnO/Fe_2O_3/Fe_3O_4$ NSs. The MO degradation of these solutions was 89% ± 1%. Errors occurred in the measurement of the quantity of $ZnO/Fe_2O_3/Fe_2O_3$ NS-containing powder, the quantity

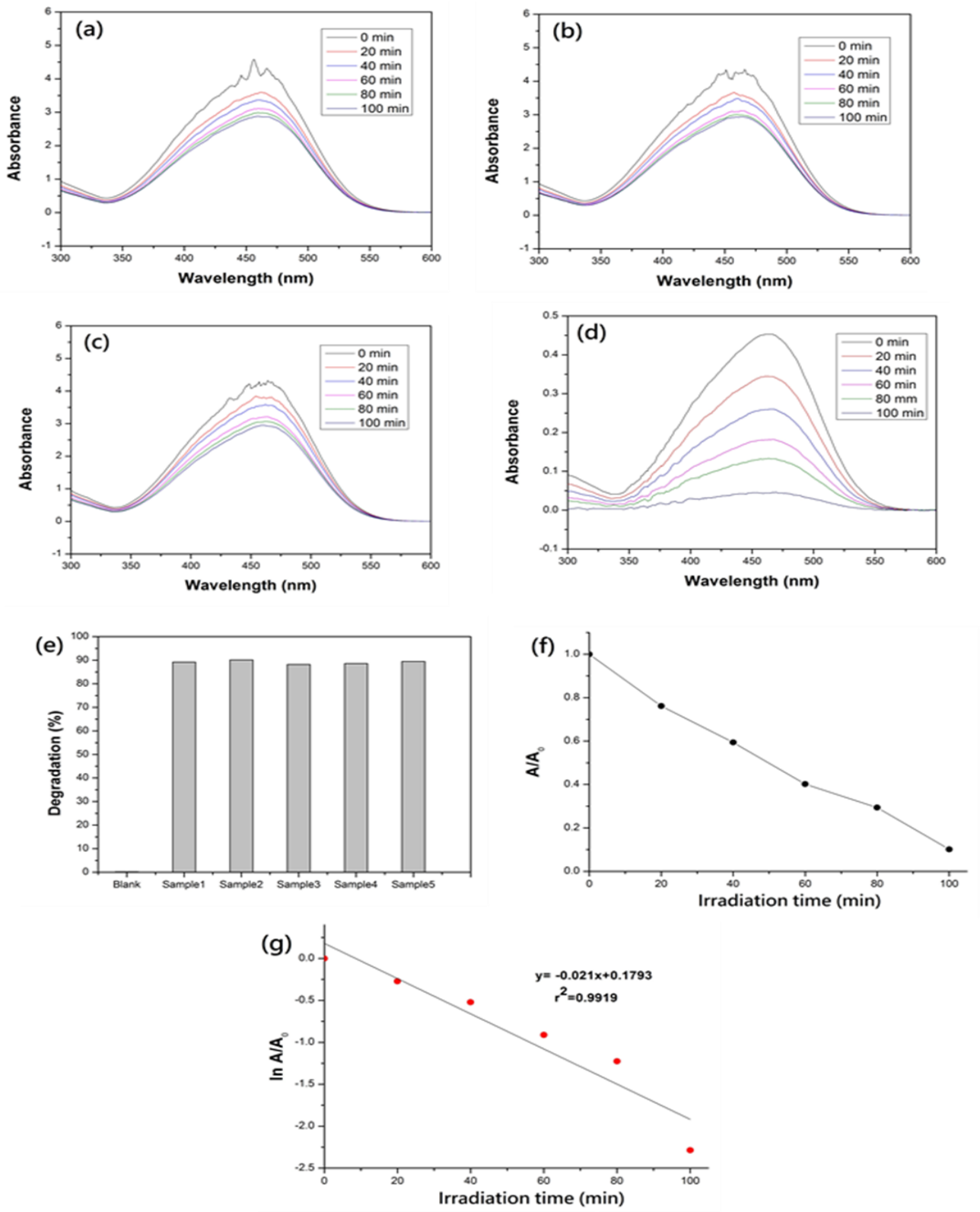

Fig. 6. (a)–(c) Absorption spectra obtained in reusability tests conducted using the $ZnO/Fe_2O_3/Fe_3O_4$ NS-containing film grown on glass for degrading MO solutions, (d) absorption spectrum of the MO solution containing 0.1 g/L of $ZnO/Fe_2O_3/Fe_3O_4$ NS-containing powder under 100-min UV illumination (MO concentration = 5 mg/L), (e) MO degradation of five MO solutions containing $ZnO/Fe_2O_3/Fe_3O_4$ NS-containing powder and an MO solution without this powder, (f) plot of A/Ao values versus radiation time for the spectrum displayed in (d), and (g) typical Langmuir–Hinshelwood plots obtained on the basis of the results shown in (f).

of MO solutions, and the UV irradiation time in Test 2; however, these errors were within an allowable range.

According to our previous research, 0.1 g/L of ZnO powder containing dandelion-like NSs can be produced at a temperature 700 °C through a two-step thermal oxidation approach. These NSs can reduce the MO concentration by almost 90% (concentration = 5 mg/L, pH = 8.1) in 120 min. [42]. The aforementioned NSs and the NSs prepared in this study exhibit a similar catalytic performance for MO; however, the synthesis temperature for ZnO dandelion-like NSs is 700 °C, whereas the synthesis temperature of the NSs prepared in this study was only 200 °C. Moreover, studies have indicated that ZnO/Fe_2O_3 NSs exhibit superior photocatalytic characteristics to bare ZnO nanorods. The enhanced photocatalytic performance of ZnO/Fe_2O_3 NSs can be attributed to the synergistic effect of ZnO and Fe_2O_3 semiconductors [43] and the effective electron–hole separation of these NSs (as indicated by the PL spectra in this study). The prepared ZnO/Fe_3O_4 NSs also exhibited magnetic properties and suitable reusability [44]. Thus, the $ZnO/Fe_2O_3/Fe_3O_4$ NSs synthesized in this study exhibited suitable photocatalytic performance.

3.2.2. Kinetic aspects of the photodegradation process

The linear imitation of dye concentration can be represented by a virtual first-order Langmuir–Hinshelwood model for heterogeneous photocatalysis, which is expressed as follows: $r = -dA/dt$ or $\ln (A/A_0) = -kt + k' (At - A_0)$, where k' is the specific reaction rate constant in mg/L min and k is the apparent first-order rate constant [45–48]. For the quantitative investigation of MO degradation, the reduction in the MO concentration (A/A_0) with irradiation time was determined for MO solutions containing $ZnO/Fe_2O_3/Fe_2O_3$ NS-containing powder [**Fig. 6(f)**]. Typical Langmuir–Hinshelwood plots were obtained from the results of **6(g)** corresponding to **6(f).** The diagram of $\ln (A/A_0)$ versus irradiation time was plotted, and the slope of this plot was 0.021 min^{-1}, which corresponds to a $t_{1/2}$ value of 30.4 min ($t_{1/2} = 0.693/k$). The obtained rate constants confirmed that the prepared $ZnO/Fe_2O_3/Fe_2O_3$ NS-containing powder is highly suitable for the mineralization of MO in polluted water.

The aforementioned results indicate that the prepared $ZnO/Fe_2O_3/Fe_2O_3$ NSs have an excellent and stable photocatalytic effect on the degradation of MO dye.

4. Conclusions

In this study, $ZnO/Fe_2O_3/Fe_3O_4$ NSs were successfully synthesized on a substrate by performing a heat treatment process in a vacuum-assisted magnetic field at 200 °C for 1 h. This method enables the rapid, simple, and low-temperature synthesis of $ZnO/Fe_2O_3/Fe_3O_4$ NSs on a substrate. The photocatalytic efficiency of the prepared NSs was tested by using them as a photocatalyst in the decomposition of MO dye under UV illumination. The experimental results indicated that a 33-mg/L $ZnO/Fe_2O_3/Fe_3O_4$ NS-containing film on a SiO substrate reduced the MO concentration by 37% (concentration = 5 mg/L, pH = 8.1) in 100 min, and the prepared $ZnO/Fe_2O_3/Fe_3O_4$ NS-containing film could be reused for MO degradation. Moreover, the experimental results indicated that 0.1 g/L of $ZnO/Fe_2O_3/Fe_3O_4$ NS-containing powder exhibited an excellent photocatalytic efficiency and reduced the MO concentration (concentration = 5 mg/L, pH = 8.1) by almost 90% in 100 min. Thus, $ZnO/Fe_2O_3/Fe_3O_4$ NSs exhibit excellent photocatalytic performance and have the potential to be used in the manufacturing of high-efficiency photocatalysts.

Acknowledgements

The authors would like to thank Naya University and Chung Young Cathay University.

References

[1]. F.K.M. Alosfur, M.H.H. Jumali, S. Radiman, N.J. Ridha, MA. Yarmo, A.A. Umar, Nanoscale Res. Lett. 8 (2013) 346.

[2]. M. I. Franch, J. A. Ayllón, J. Peral and X. Domènech, Appl. Catal. B: Environ. 50 (2004) 89-99.

[3]. S. Senobari, A. Nezamzadeh-Ejhieh, Acta Part A: Molecul. Biomolecul. Spect. 196 (2018) 334–343.

[4]. S. H. Lin and R. S. Juang, J. Environ. Manage. 90 (2009) 1336-1349.

[5]. S.B. Wang and Y.L. Peng, Chem. Eng. J. 156 (2010) 11-24.

[6]. P. Patil, G. Gaikwad, D.R. Patil and J. Naik, Bull. Mater. Sci. 39 (2016) 655-665.

[7]. Y.C. Lu, C.C. Chang and C.S. Lu, J. Taiwan Inst. Chem. Eng. 45 (2014) 1015-1024.

[8]. M. Hafizuddin, H. Jumali, F.K.M. Alosfur, S. Radiman, N.J. Ridha, M.A. Yarmo, A.A. Umar, Materi. Sci. in Semi. Proces. 25 (2014) 207-210.

[9]. S. Phanichphant, A. Nakaruk, K. Chansaenpak, D. Channei, Scientific Rep. 9 (2019) 16091.

[10]. A. Mclaren, T. Valdes-Solis, G.Q. Li and S.C. Tsang, J. Am. Chem. Soc. 131 (2009) 12540-12541.

[11]. H. Hassena, Mod. Chem. Appl. 4 (2016) 1000176.

[12]. P.D. Yang, R.X. Yan, M. Fardy, Nano Lett. 10 (2010) 1529-1536.

[13]. M.A. Subhan, A.M.M. Fahim, P.C. Saha, M.M. Rahman, K. Begum, A.K. Azad, Nano-Str. & Nano-Obj. 10 (2017) 30-41.

[14]. Q. Zhou, J.Z. Wen, P. Zhao and W.A. Anderson, Nanomaterials 7 (2017) 9.

[15]. S. Xia, Y. Meng, X. Zhou, J. Xue, G. Pan, Z. Ni, Appl. Cata. Env. 187 (2016) 122-133.

[16]. L. Vayssieres, Adv. Mater. 15 (2003) 464-466.

[17]. Q.Q. Xiong, X.H. Xia, J.P. Tu, J. Chen, Y.Q. Zhang, D. Zhou, C.D. Gu, X.L. Wang, J. Powe. Sour. 240 (2013) 344-350.

[18]. Y.L. Chueh, M.W. Lai, J.Q. Liang, L.J. Chou, Z.L. Wang, Adv. Func. Mate. 16 (2006) 2243-2251.

[19]. S.Y. Li, C.Y. Lee, T.Y. Tseng, J. Crysta. Grow .247 (2003) 357-362.

[20]. J.Y. Park, Y.S. Yen, Y.S. Hong, H. Oh, J.J. Kim, S.S. Kim, Composites: Part B 37 (2006) 408-412.

[21]. H.B.A. Kadhim, N.J. Ridha, F.K.M. Alosfur, N.M Umran, R. Madlol, K. Tahir and R.T. Ahmed, J. Physics: Conf. Series 1032 (2018) 012039.

[22]. W.T. Chiou, W.Y. Wu, J.M. Ting, Diam. Relat. Mater. 12 (2003) 1841-1844.

[23]. T.J. Kuo, C.N. Lin, C.L. Kuo, M.H. Huang, Chem. Mater. 19 (2007) 5143-5147.

[24]. Q. Li, Q. Wang, Z. Chen,Q. Ma, M. An, Nanomaterials 9 (2019) 846.

[25]. N.F. Hsu, T.K. Chung, M. Chang, H.J. Chen, J. Mater. Sci. Technol. 29 (2013) 893-897.

[26]. N.F. Hsu, M. Chang, Mater. Chem. Phys. 135 (2012) 112-116.

[27]. J. Zhang, N. Li, Oxidation mechanism of steels in liquid–lead alloys, Oxidation of Metals 63 (2005) 353-381.

[28]. M. Ohring, The materials science of thin films, 2nd Edn., Academic Press, San Diego, 2002. pp. 357-415.

[29]. M. Chang, N.F. Hsu, Chin. J. Chem. Phys. 24 (2011) 109-114.

[30]. B. Jia, L. Gao, J. Phys. Chem. C 112 (2008) 666-671.

[31]. H. Derikvandi, A. Nezamzadeh-Ejhieh, J. Molecul. Catal. A: Chem. 426 (2017) 158–169.

[32]. X. Zhang, L. Wang, G. Zhou, Rev. Adv. Mater. Sci. 10 (2005) 69-72.

[33]. D. Behera, B.S. Acharya, J. Lumi. 128 (2008) 1577-1586.

[34]. X.D. Gao, X.M. Li, W.D. Yu, J. Sol. State. Chem. 177 (2004) 3830-3834.

[35]. K. Vanheusden, W.L. Warren, C.H. Seager, D.R. Tallant, J.A. Voigt, B.E. Gnade, J. Appl. Phys. 79 (1996) 7983-7990.

[36]. X.L. Wu, G.G. Siu, C.L. Fu, H.C. Ong, Appl. Phys. Lett. 78 (2001) 2285-2287.

[37]. Q. Qi, T. Zhang, Q. Yu, R. Wang, Y. Zeng, L. Liu, H. Yang, Sens. Actuat B: Chem. 133 (2008) 638-643.

[38]. J. Al-Sabahi, T. Bora, M. Al-Abri and J. Dutta, Materials 9 (2016) 238.

[39]. X. Zhang, J. Qin, Y. Xue, P. Yu, B. Zhang, L. Wang, R. Liu, Sci. Rep. 4 (2014) 4596.

[40]. S. Bhatia and N.Verma, Mater. Res. Bull. 95 (2017) 468-476.

[41]. F.M. Meng, X.P. Song, Z.Q. Sun, Vacuum 83 (2009) 1147-1151.

[42]. N.F. Hsu, M. Chang, K.T. Hsu, Mater. Sci. in Semi. Proce. 21 (2014) 200-205.

[43]. Y. Liu, L. Sun, J. Wu, T. Fang, R.Cai, A. Wei, Mater.Sci. and Eng.: B 194 (2015) 9-13.

[44]. J.C. Sin, S.Q. Tan, J.A. Quek, S.M. Lam, A.R. Mohamed, Mater. Lett.228, (2018) 207-211.

[45]. A. Nezamzadeh-Ejhieh, S. Hushmandrad, Appl.Catal.A: Gene. 388 (2010) 149-159.

[46]. S. Ghattavi, A. Nezamzadeh-Ejhieh, Inter. J. Hydro. Ene.. 45 (2020) 24636-24656.

[47]. B. Manikandan, K.R. Murali, R. John, Iran. J. of Catal. 11(1) (2021) 1-11.

[48]. M. Mehrali-Afjania, A.Nezamzadeh-Ejhieha, H. Aghaei, Chem. Phys. Lett. 759 (2020) 137873.